Implementation of a multi-axial pseudoelastic model to predict the dynamic behavior of shape memory alloys

F Thiebaud, M Collet, E Foltete and C Lexcellent

Institut Femto-ST, UMR CNRS 6174, Départment LMARC, 24 Chemin de l'Epitaphe 25000, Besancon, France

E-mail: Christian.Lexcellent@univ-fcomte.fr

Abstract
Shape memory alloys (SMAs) are good candidates for being used as passive dampers, strain sensors, stiffness or shape drivers. In order to develop the use of these alloys in structural vibration control, we present in this paper an implementation of a phenomenological model based on the R_l model (Raniecki *et al* 1992 *Arch. Meh.* **44** 261–84) in a finite element code called COMSOL© which allows one to build automatically many loading cases in force or displacement. This implementation is used to simulate internal loops in order to characterize the stiffness and the damping effect by an equivalent complex Young's modulus approach under static strain offsets. The results clearly show the influence of the initial static strain offset and the amplitude of vibration on the damping and stiffness properties.

1. Introduction

Shape memory alloys (SMAs) are widely studied as smart materials because of their potentiality to be used as dampers, absorbers or actuator elements. For damping applications, an understanding of the material dynamic behavior is needed. One uses the loss of stiffness linked to the martensite transformation between the mother phase called austenite and the product phase called martensite. The process of reorientation of martensite platelets sometimes called pseudoplasticity can also be used. In this case, the SMA elements are used as absorbers mainly for seismic applications [2–4]. The best example of structural control by SMAs can be found in the basilic St Francois d'Assise in Italy.

For technological applications, the effect of a static strain offset on the dynamic response of a system is investigated. In order to evaluate the stiffness and damping evolutions during the martensite transformation, a method based on an equivalent complex Young's modulus determination [5, 6] is initiated.

In the present paper, first a phenomenological model at the macroscopic scale in the framework of the thermodynamics of irreversible processes devoted to multi-axial pseudoelasticity [1] initiated by Raniecki *et al* called the R_l model [1] is recalled.

In the second part, this model is implemented in a finite element code. The software COMSOL© has been chosen because of its facilities for solving multiphysic coupled problems which is the case for phase transitions linked to dynamic loadings. In order to validate the implementation, some tests are performed: plate in tension, plate in bi-tension, plate under bending in its plane.

In the third part, the equivalent complex Young's modulus method is quickly described and the stiffness and damping evolutions are investigated.

2. A thermomechanical model for the pseudoelasticity

Modeling material behavior needs classically the choice of a thermodynamic potential (free energy or free enthalpy expression) and also a dissipation potential function or some yield functions of the phase transformation (as is the scheme

in plasticity). Hence, a Helmholtz free energy and two yield functions, the first for the forward phase transformation ($A \rightarrow M$) and the second for the reverse phase transformation ($M \rightarrow A$), are chosen. The model initiated by Raniecki *et al* [1] has been written in order to describe multi-axial loading.

The appropriate internal variable is the volume fraction of martensite M: ξ ($(1-\xi)$ being the volume fraction of austenite A).

The free energy function of the two phases ($A + M$) in the representative elementary volume (REV) is chosen as

$$\begin{aligned}\phi(\underline{\varepsilon}, T, \xi) &= u_0^1 - Ts_0^1 - \xi \times \pi_0^{\mathrm{f}}(T) \\ &+ \tfrac{1}{2}(\underline{\varepsilon} - \underline{\varepsilon}^{\mathrm{tr}}) : \underline{\underline{L}} : (\underline{\varepsilon} - \underline{\varepsilon}^{\mathrm{tr}}) \\ &- C_v \ln\left(\frac{T}{T_0}\right) + \xi(1-\xi)\phi_{it} \end{aligned} \tag{1}$$

where $\pi_0^{\mathrm{f}}(T)$ represents the thermodynamic driving force associated with the phase transformation in the stress free state:

$$\pi_0^{\mathrm{f}}(T) = \Delta u^* - T\Delta s^* \tag{2}$$

where $\Delta u^* = u_0^1 - u_0^2$ and $\Delta s^* = s_0^1 - s_0^2$ represent the differences between the internal energy and entropy of austenite and martensite respectively with:

$\underline{\varepsilon}$: strain tensor (small deformation hypothesis),
$\underline{\varepsilon}^{\mathrm{tr}}$: phase transformation strain tensor,
ξ: volume fraction of martensite M,
$1-\xi$: volume fraction of austenite A,
T: temperature (K),
T_0: reference temperature (K),
$\underline{\underline{L}}$: elastic stiffness tensor,
C_v: specific heat.

The exact form of $\Delta\phi$ remains an open problem since it strongly depends on the incompatibilities between the martensite platelets themselves and between these platelets and the mother phase A. The simplest expression which disappears when the system is single phase is chosen as

$$\Delta\phi = \xi(1-\xi)\phi_{it}(T) \tag{3}$$

where

$$\phi_{it} = \overline{u}_0 - T\overline{s}_0. \tag{4}$$

Sometimes, $\overline{u}_0$ ($\overline{s}_0$) is called the internal configurational energy (entropy). In a classical way, the Cauchy stress tensor can be obtained as

$$\underline{\sigma} = \rho\frac{\partial\phi}{\partial\underline{\varepsilon}} = \underline{\underline{L}}(\underline{\varepsilon} - \underline{\varepsilon}^{\mathrm{tr}}). \tag{5}$$

For the phase transformation strain tensor, an expression not far from the plasticity is chosen:

$$\underline{\varepsilon}^{\mathrm{tr}} = \frac{3}{2}\frac{\mathrm{dev}(\underline{\sigma})}{\overline{\sigma}}\gamma\xi \tag{6}$$

$\mathrm{dev}(\underline{\sigma})$ represents the deviatoric stress tensor with the natural definition:

$$\mathrm{dev}(\underline{\sigma}) = \underline{\sigma} - \tfrac{1}{3}\mathrm{tr}(\underline{\sigma})Id \tag{7}$$

$$\Rightarrow \mathrm{tr}(\mathrm{dev}(\underline{\sigma})) = 0 \tag{8}$$

$$\text{with } \overline{\sigma} = (\tfrac{3}{2}\mathrm{dev}(\underline{\sigma}) : \mathrm{dev}(\underline{\sigma}))^{1/2}. \tag{9}$$

This choice means that the phase transformation does not depend on an isotropic loading such as pressure. It emerges that the phase transformation is isochoric (like the plastic transformation).

With the expression (6), one cannot take into account the asymmetry between tension and compression. A more convenient expression has been stated by Raniecki *et al* [7] and will be implemented soon.

If one defines the phase transformation equivalent strain $\overline{\varepsilon}_{\mathrm{tr}}$, as usual:

$$\overline{\varepsilon^{\mathrm{tr}}} = \left(\tfrac{2}{3}\mathrm{dev}(\underline{\varepsilon}^{\mathrm{tr}}) : \mathrm{dev}(\underline{\varepsilon}^{\mathrm{tr}})\right)^{1/2} \tag{10}$$

it can be written that

$$\overline{\varepsilon^{\mathrm{tr}}} = \gamma\xi. \tag{11}$$

The thermodynamic driving force associated with the progress of the phase transformation can be written as

$$\pi^{\mathrm{f}}(\underline{\sigma}, \xi, T) = -\frac{\partial\phi}{\partial\xi} = \frac{\gamma\overline{\sigma}}{\rho} + \pi_0^{\mathrm{f}}(T) - (1-2\xi)\phi_{it}(T). \tag{12}$$

A classical calculation delivers the expression for the increment of dissipation $\mathrm{d}D$ which cannot be negative:

$$\mathrm{d}D = \pi^{\mathrm{f}}\mathrm{d}\xi \geqslant 0. \tag{13}$$

Thus, the present inequality precludes the forward phase transformation ($A \rightarrow M$) only if $\pi^{\mathrm{f}} \geqslant 0$ and the reverse one if $\pi^{\mathrm{f}} \leqslant 0$. One has to note that $\pi^{\mathrm{f}} = 0$ implies the equilibrium condition. In order to specify the kinetic equations driving the phase transformation, we assume the existence of two functions $\psi^\alpha(\pi^{\mathrm{f}}, \xi)(\alpha = 1, 2)$ such that an active process of parent phase decomposition ($A \rightarrow M : \mathrm{d}\xi > 0$) can only proceed when $\psi^1 = \text{const}$, ($\mathrm{d}\psi^1 = 0$) and an active process of martensite decomposition ($M \rightarrow A : \mathrm{d}\xi < 0$) can only proceed if $\psi^2 = \text{const}$, ($\mathrm{d}\psi^2 = 0$). These yield functions are chosen as

$$\psi^1 = \pi^{\mathrm{f}} - k^{(1)}(\xi) \tag{14}$$

$$\psi^2 = -\pi^{\mathrm{f}} + k^{(2)}(\xi). \tag{15}$$

The expressions for $k^\alpha(\xi)$ are built to give kinetics in agreement with the measurements of metallurgists such as Koistinen and Marbuger [8]:

$$k^{(1)}(\xi) = -A_1\ln(1-\xi) \tag{16}$$

$$k^{(2)}(\xi) = A_2\ln(\xi). \tag{17}$$

Thanks to the derivation, the kinetic laws for forward and reverse phase transformations are obtained (for isothermal external conditions ($\dot{T} = 0$)):

$$\dot{\xi}_{A\rightarrow M}(\dot{\overline{\sigma}}, \xi) = \frac{\frac{\gamma\dot{\overline{\sigma}}}{\rho}}{\frac{A_1}{1-\xi} - 2\phi_{it}(T)} \tag{18}$$

$$\dot{\xi}_{M\rightarrow A}(\dot{\overline{\sigma}}, \xi) = \frac{\frac{\gamma\dot{\overline{\sigma}}}{\rho}}{\frac{A_2}{\xi} - 2\phi_{it}(T)}. \tag{19}$$

Moreover, the calculations deliver a relation between the two classical Von Mises invariants $\overline{\sigma}$ and $\overline{\varepsilon}$:

Table 1. Both displacement and force formulations.

Displacement control	Force control
Von Mises equivalent strain and stress $\overline{\varepsilon}$ and $\overline{\sigma}$	
$\overline{\varepsilon} = (\frac{2}{3}\mathrm{dev}(\underline{\varepsilon}) : \mathrm{dev}(\underline{\varepsilon}))^{1/2}$	$\overline{\sigma} = (\frac{3}{2}\mathrm{dev}(\underline{\sigma}) : \mathrm{dev}(\underline{\sigma}))^{1/2}$
Relation between $\overline{\sigma}$ and $\overline{\varepsilon}$	
$\overline{\varepsilon} = \frac{2(1+\upsilon)}{3E}\overline{\sigma} + \gamma\xi$	$\overline{\sigma} = \frac{3E}{2(1+\upsilon)}(\overline{\varepsilon} - \gamma\xi)$
Thermodynamic driving force π_{f}	
$\pi_{\mathrm{f}}(\overline{\varepsilon}, \xi, T) = \frac{3\gamma E}{2\rho(1+\nu)}\overline{\varepsilon} + \pi_{\mathrm{f}}^0(T)$ $-(1-2\xi)\phi_{it}(T) - \frac{3\gamma^2 E}{2\rho(1+\nu)}\xi$	$\pi_{\mathrm{f}}(\overline{\sigma}, \xi, T) = \frac{\gamma}{\rho}\overline{\sigma} + \pi_{\mathrm{f}}^0(T)$ $-(1-2\xi)\phi_{it}(T)$
Forward phase transformation $\dot{\xi}_1$	
$\dot{\xi}_1(\dot{\overline{\varepsilon}}, \xi, T) = \frac{3\gamma E\dot{\overline{\varepsilon}}}{2\rho(1+\upsilon)(\frac{A_1}{1-\xi} - 2\phi_{it}(T)) + 3\gamma^2 E}$	$\dot{\xi}_1(\dot{\overline{\sigma}}, \xi, T) = \frac{\frac{\gamma\dot{\overline{\sigma}}}{\rho}}{\frac{A_1}{1-\xi} - 2\phi_{it}(T)}$
Reverse phase transformation $\dot{\xi}_2$	
$\dot{\xi}_2(\dot{\overline{\varepsilon}}, \xi, T) = \frac{3\gamma E\dot{\overline{\varepsilon}}}{2\rho(1+\upsilon)(\frac{A_2}{\xi} - 2\phi_{it}(T)) + 3\gamma^2 E}$	$\dot{\xi}_2(\dot{\overline{\sigma}}, \xi, T) = \frac{\frac{\gamma\dot{\overline{\sigma}}}{\rho}}{\frac{A_2}{\xi} - 2\phi_{it}(T)}$

$$\overline{\sigma} = \frac{3E}{2(1+\upsilon)}(\overline{\varepsilon} - \gamma \cdot \xi) \tag{20}$$

with

$$\overline{\varepsilon} = \left(\tfrac{2}{3}\mathrm{dev}(\underline{\varepsilon}) : \mathrm{dev}(\underline{\varepsilon})\right)^{1/2}. \tag{21}$$

The relation (20) allows us to write the thermodynamic driving force as a function of the strain invariant $\overline{\varepsilon}$, ξ, T and the kinetic laws as functions of $\dot{\overline{\varepsilon}}$ and ξ:

$$\pi_{\mathrm{f}}(\overline{\varepsilon}, \xi, T) = \frac{3\gamma E}{2\rho(1+\nu)}\overline{\varepsilon} + \pi_{\mathrm{f}}^0(T) - (1-2\xi)\phi_{it}(T) - \frac{3\gamma^2 E}{2\rho(1+\nu)}\xi \tag{22}$$

and

$$\dot{\xi}_{A\to M}\left(\dot{\overline{\varepsilon}}, \xi, T\right) = \frac{3\gamma E\dot{\overline{\varepsilon}}}{2\rho(1+\upsilon)\left(\frac{A_1}{1-\xi} - 2\phi_{it}(T)\right) + 3\gamma^2 E} \tag{23}$$

$$\dot{\xi}_{M\to A}(\dot{\overline{\varepsilon}}, \xi, T) = \frac{3\gamma E\dot{\overline{\varepsilon}}}{2\rho(1+\upsilon)\left(\frac{A_2}{\xi} - 2\phi_{it}(T)\right) + 3\gamma^2 E}. \tag{24}$$

These two alternative formulations allow us to solve the problem when the input variables are the stress rate tensor $\dot{\underline{\sigma}}$ (output: displacement) or the displacement rate $\dot{\overrightarrow{u}}$ (output: stress state). An assessment of these formulations is given in table 1:

3. Implementation in COMSOL©

COMSOL© is a modeling package for the simulation of any physical process and can be described with partial differential equations (PDEs). It features state-of-the-art solvers that address complex problems quickly and accurately, while its intuitive structure is designed to provide ease of use and flexibility. This software is chosen for its ability to build automatically some cycles and internal loops. The R_l model described in section 2 has been implemented for 2D problems with plane stress assumptions. It can be applied to a multiphysic coupled problem with a structural mechanics module (for the mechanical behavior) and a PDE module (for the kinetic transformations).

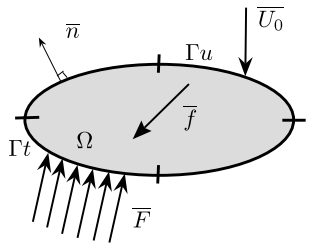

Figure 1. Domain Ω and boundary conditions.

This section converts the 'translation' of the R_L model for plane stress problems into characteristic equations to be implemented in COMSOL©.

3.1. Principle of virtual work

The principle of virtual work expressed in global stress components states that the sum of virtual works from internal strains are equal to the works from external loads. This principle will be applied under the following assumptions:

- small disturbances,
- the inertial terms are not taken into account; i.e. the steady state response is considered,
- due to the steady state response considerations, the temperature variations are neglected, and thus an isothermal behavior ($T = T_0$) is considered; a more convenient adiabatic behavior has been stated by Lexcellent *et al* [9] and will be implemented in a future work.

Let us consider a continuous domain Ω, loaded with force $\overline{F}/\,\Gamma_t$ or displacement $\overline{U_0}/\,\Gamma_u$. $\overline{f}$ represents the volumic force and $\overline{n}$ the outgoing perpendicular vector.

The total stored energy $\mathcal{W}$ from the external and internal strains and loads is

$$\mathcal{W}(\mathbf{u}^*) = -\tfrac{1}{2}\int_\Omega \mathrm{tr}[\underline{\sigma}.\underline{\varepsilon}(\mathbf{u}^*)]\,\mathrm{d}\Omega + \int_\Omega \overline{\mathbf{f}}.\mathbf{u}^*\mathrm{d}\Omega + \int_{\Gamma t} \overline{\mathbf{F}}.\mathbf{u}^*\mathrm{d}\Omega \tag{25}$$

where $\mathbf{u}^*$ belongs to the whole of the kinematically admissible fields defined by

$$\mathcal{U}_{\mathrm{ad}} = \left\{\mathbf{u}^* \in H_1 / \mathbf{u}^* = \overline{\mathbf{U}}_0 \text{ on } \Gamma u\right\} \tag{26}$$

and

$$\underline{\sigma}(\mathbf{n}) = \overline{\mathbf{F}} \qquad \text{on } \Gamma t. \tag{27}$$

Thus, the principle of virtual work states that

$$\mathrm{d}\mathcal{W} = 0. \tag{28}$$

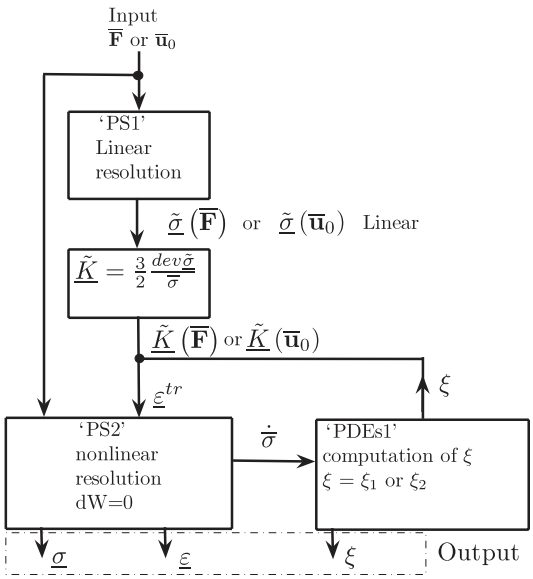

Figure 2. Diagram of the interactions between the three modules 'PS1', 'PS2' and 'PDEs1'.

3.2. Implementation

In order to calculate $\mathcal{W}$, the stress tensor $\underline{\sigma}$, the solution of the multiphysic problem, must be evaluated in the COMSOL© scalar expressions. This can be done by considering both equations (5) and (6):

$$\underline{\sigma} = \underline{\underline{L}}(\underline{\varepsilon}(\mathbf{u}) - \underline{K}(\underline{\sigma})\gamma\xi) \tag{29}$$

where $\underline{K}$ is a tensor defined by

$$\underline{K}(\underline{\sigma}) = \frac{3}{2}\frac{\mathrm{dev}(\underline{\sigma})}{\overline{\sigma}}. \tag{30}$$

The equation (29) appears as an implicit expression for $\underline{\sigma}$, $\left(\underline{\sigma} = f\left(\underline{\varepsilon}(\mathbf{u}), \underline{\sigma}\right)\right)$, which is incomprehensible for COMSOL©. The value of K_{ij} depends on the boundary conditions, loadings and finally the problem investigated.

In the case of force loadings (displacement loadings), a tensor $\underline{\tilde{K}}$ is obtained by the elastic resolution of Neumann's problem (Dirichlet's problem). This elastic resolution is typically done by a 'structural mechanical module' called 'PS1'. If $(\underline{\tilde{\sigma}}, \underline{\tilde{\varepsilon}})$ is the elastic solution obtained by this module, the equation (29) becomes

$$\underline{\sigma} = \underline{\underline{L}}(\underline{\varepsilon}(\mathbf{u}) - \underline{\tilde{K}}\gamma\xi) \tag{31}$$

where

$$\underline{\tilde{K}} = \frac{3}{2}\frac{\mathrm{dev}(\underline{\tilde{\sigma}})}{\overline{\tilde{\sigma}}}. \tag{32}$$

In this way, the implicit problem (equation (29)) is transformed into the explicit problem (equation (31)), which is easily implemented in COMSOL©.

Finally, three modules are used to solve the multiphysic problem:

- 'structural mechanics 1' (PS1): elastic resolution, construction of the components $\tilde{K}_{ij}$ of $\tilde{K}$,
- 'structural mechanics 2' (PS2): nonlinear resolution, construction of the multiphysic problem where the solution is $\underline{\sigma}$ and $\mathbf{u}$,
- 'partial differential equation 1' (PDEs1): nonlinear coupling with PS2. Calculation of the increment or decrement of ξ.

The diagram given in figure 2 shows the interactions between these three modules. The computation of $\underline{\tilde{K}}$ and ξ (at each time of the process) gives $\underline{\varepsilon}^{\mathrm{tr}}$ and allows the nonlinear resolution of equation (28).

3.3. Case of plane stress

By considering the plane stress assumptions (corresponding to a plate under 'ad hoc' loading conditions), the stress tensor is clearly defined by

$$\underline{\sigma} = \begin{bmatrix} \sigma_{11} & \sigma_{12} & 0 \\ \sigma_{12} & \sigma_{22} & 0 \\ 0 & 0 & 0 \end{bmatrix}. \tag{33}$$

Thus, the tensor $\underline{\tilde{K}}$ can be given explicitly as

$$\underline{\tilde{K}} = \frac{1}{2\overline{\tilde{\sigma}}}\begin{bmatrix} 2\tilde{\sigma}_{11} - \tilde{\sigma}_{22} & 3\tilde{\sigma}_{12} & 0 \\ 3\tilde{\sigma}_{12} & 2\tilde{\sigma}_{22} - \tilde{\sigma}_{11} & 0 \\ 0 & 0 & -(\tilde{\sigma}_{11} + \tilde{\sigma}_{22}) \end{bmatrix} \tag{34}$$

with

$$\overline{\tilde{\sigma}} = \left(\tilde{\sigma}_{11}^2 + \tilde{\sigma}_{22}^2 + 3\tilde{\sigma}_{12}^2 - \tilde{\sigma}_{11}^2\tilde{\sigma}_{22}^2\right)^{1/2}. \tag{35}$$

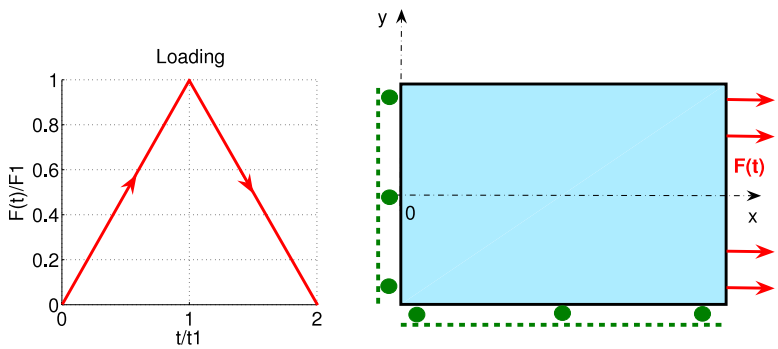

Figure 3. Force loading and boundary conditions for a plate in tension.

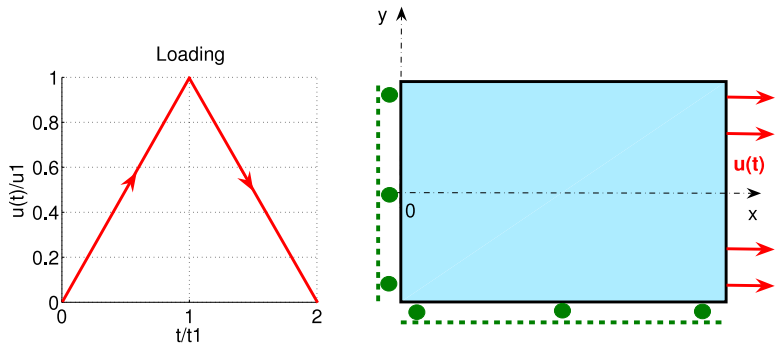

Figure 4. Displacement loading and boundary conditions for a plate in tension.

The partition of the total strain into an elastic part and phase transformation part is recalled:

$$\underline{\varepsilon} = \underline{\varepsilon}^{\mathrm{el}} + \underline{\varepsilon}^{\mathrm{tr}} \tag{36}$$

and the elastic strain tensor can be clarified as

$$\underline{\varepsilon}^{\mathrm{el}} = \begin{bmatrix} \varepsilon_{11} - \tilde{K}_{11}\gamma\xi & \varepsilon_{12} - \tilde{K}_{12}\gamma\xi & 0 \\ \varepsilon_{12} - \tilde{K}_{12}\gamma\xi & \varepsilon_{22} - \tilde{K}_{22}\gamma\xi & 0 \\ 0 & 0 & \varepsilon_{33}^{\mathrm{el}} \end{bmatrix} \tag{37}$$

with

$$\varepsilon_{33}^{\mathrm{el}} = -\frac{\nu}{1-\nu}\left(\varepsilon_{11}^{\mathrm{el}} + \varepsilon_{22}^{\mathrm{el}}\right). \tag{38}$$

4. Results

Before investigating the dynamic behavior of SMAs by the equivalent complex Young's modulus approach, many static tests were performed in order to validate the implementation presented in section 3.

One nonhomogeneous and two homogeneous tests are presented: a plate in tension (with both cases of force and displacement loadings), a plate in proportional bi-tension and a plate in bending loaded in its plane. This last test shows the ratio of martensite at each time of the process and each test point $A(x, y)$ in the plate.

4.1. Design of the plate

The static tests are performed for a rectangular plate. Its dimensions are: length $L = 80$ mm, width $l = 40$ mm and thickness $e = 10$ μm. The SMA used in the numerical application is CuAlBe. Its characteristic phase transformation temperatures derived from electrical resistance measurements are: $M_{\mathrm{f}}^0 = 191$ K, $M_{\mathrm{S}}^0 = 213$ K, $A_{\mathrm{S}}^0 = 205$ K, $A_{\mathrm{F}}^0 = 221$ K. The material parameters are: $E = 7.5 \times 10^{10}$ Pa, $\rho = 8129$ kg m^{-3}, $\Delta u^* = 2871.6$ J m^{-3}, $\Delta s^* = 11$ J m^{-3}, $u_0 = 100.3$ J m^{-3}, $\gamma = 0.0295$, $\alpha = 0.055$, $C_v = 490$ J kg^{-1}, $\alpha_0 = 17 \times 10^{-6}$ K^{-1}. These parameters have been identified by performing classical tensile tests at different temperatures in the range of pseudoelasticity, as described in [7].

4.2. Plate in tension

The plate is loaded (in force or displacement, figures 3 and 4) for one cycle in order to observe the forward transformation

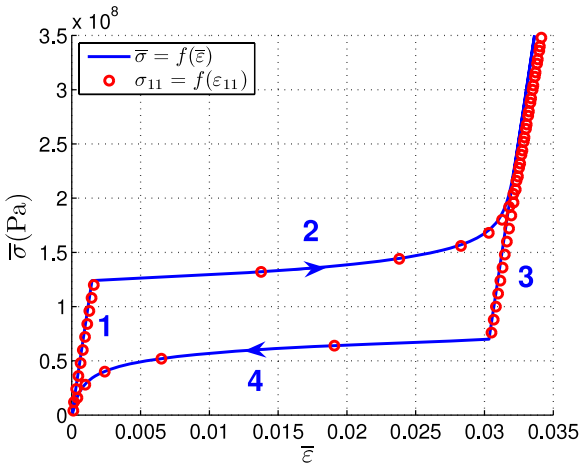

Figure 5. Force loading: $\overline{\sigma}$ versus $\overline{\varepsilon}$ and σ_{11} versus ε_{11} for a plate in tension at $T = 293$ K.

($A \rightarrow M$) and the reverse transformation ($M \rightarrow A$):

$$F : t \mapsto -\dot{F} \cdot (|t - t_1| + t_1) \tag{39}$$

$$u : t \mapsto -\dot{u} \cdot (|t - t_1| + t_1) \tag{40}$$

where $\dot{F}$ and $\dot{u}$ are the rates of loading and t_1 the instant of the end of the loading. t_1 is chosen in order to observe a complete forward transformation.

Note that the values of $\dot{F} = 1$ N s^{-1} and $\dot{u} = 1$ μm s^{-1} are arbitrarily chosen as the problem is not time dependent, due to the assumption of quasi-static behavior.

The Von Mises stress $\overline{\sigma}$ evolution versus $\overline{\varepsilon}$ is given in figures 5 and 6 as well as the normal stress σ_{11} versus ε_{11}. It can be verified that the four steps of the material response are present:

- step 1: elastic behavior of the austenite,
- step 2: forward transformation $A \rightarrow M$,
- step 3: elastic behavior of the martensite,
- step 4: reverse transformation $M \rightarrow A$.

The two curves shown in those figures are the same because the R_I model is an 'as plasticity' one or independent time model. Thus, the typical pseudoelastic behavior is obtained.

It can be interesting to represent fundamental quantities of the model like the thermodynamic driving force π_{f} (figure 7

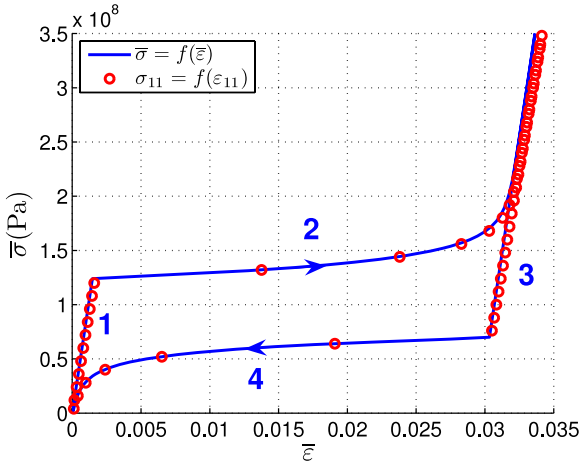

Figure 6. Displacement loading: $\overline{\sigma}$ versus $\overline{\varepsilon}$ and σ_{11} versus ε_{11} for a plate in tension at $T = 293$ K.

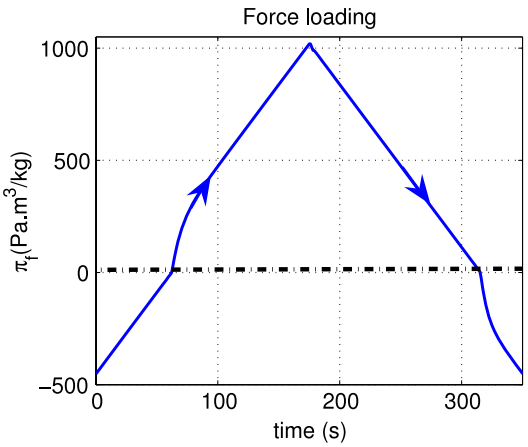

Figure 7. Force loading: π_f versus the time t.

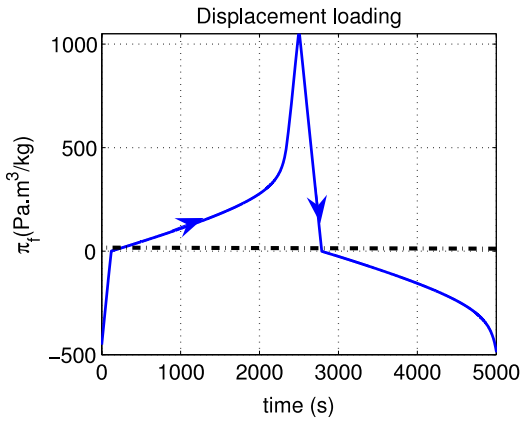

Figure 8. Displacement loading: π_f versus the time t.

and 8) and the volume fraction of martensite ξ (figure 9 and 10) versus the time t.

When π_f becomes positive, in the loading phase, the forward transformation is beginning: $\xi \to 1$. A variation of the slope of π_f is noticed. Indeed, the increment of π_f versus

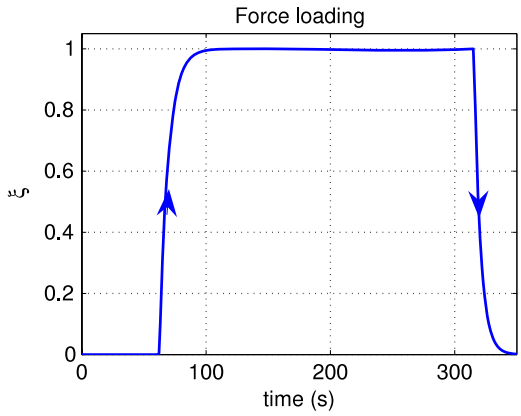

Figure 9. Force loading: ξ versus the time t.

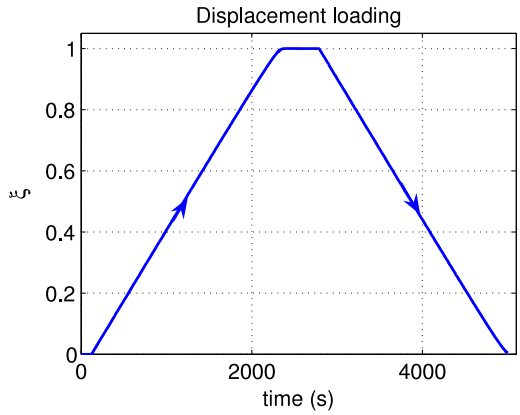

Figure 10. Displacement loading: ξ versus the time t.

the time is given by

$$\frac{\mathrm{d}\pi_f}{\mathrm{d}t}(\dot{\overline{\sigma}}, \dot{\xi}, T) = \frac{\gamma\dot{\overline{\sigma}}}{\rho} + 2\dot{\xi}\phi_{it}(T) \tag{41}$$

for the force loading, and

$$\frac{\mathrm{d}\pi_f}{\mathrm{d}t}(\dot{\overline{\varepsilon}}, \dot{\xi}, T) = \frac{3E\gamma\dot{\overline{\varepsilon}}}{2\rho(1+\nu)} + 2\dot{\xi}\phi_{it}(T) - \frac{3E\gamma}{2\rho(1+\nu)}\dot{\xi} \tag{42}$$

for the displacement loading.

Hence, when the forward transformation begins, the dependent factors of $\dot{\xi}$ affect the increment of π_f respectively in force and displacement loadings.

When π_f becomes negative, in the unloading phase, the reverse transformation is beginning ($\xi \to 0$). As previously, a variation of slope is observed. It can be noticed that the time t is only one parameter which makes it possible to follow the movement.

4.3. Plate in proportional bi-tension

A plate loaded in force in proportional bi-tension is now studied (figure 11). Experimentally, this device allows one to effect the training of SMAs as described in [10] and [11]. The coefficient K represents the coefficient of proportionality between the force on the (0, **x**) axis and the force on the (0, **y**)

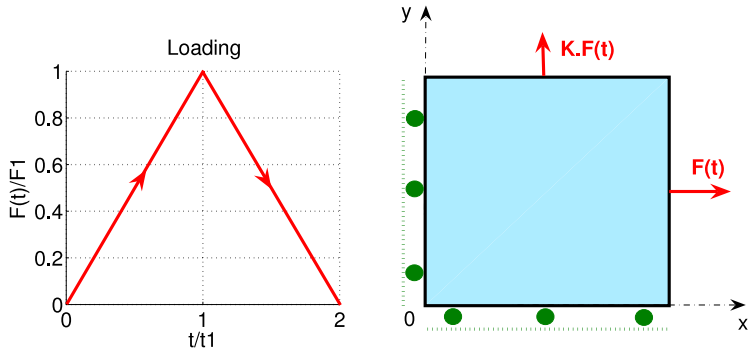

Figure 11. Force loading: plate in proportional bi-tension.

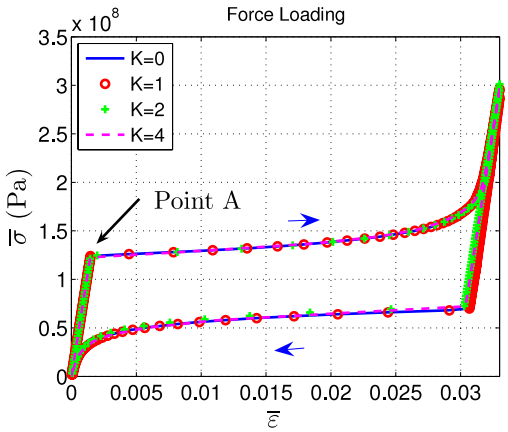

Figure 12. Force loading: plate in proportional bi-tension.

axis ($K = \sigma_{22}/\sigma_{11}$). Many simulations have been done with $K = 0, 0.5, 1, 1.5$.

Hence, the Von Mises stress $\overline{\sigma}$ evolution versus $\overline{\varepsilon}$ is given for different values of K on figure 12. The beginning point (point A) of the forward transformation ($A \rightarrow M$) is the same for each simulation (each value of K).

Due to equation (20), the curves are the same for each value of K. An increase of $\overline{\sigma}$ is noticed when K increases which is due to the relation between σ_{11} and $\overline{\sigma}$:

$$\overline{\sigma} = (1 + K^2 - K)^{1/2}\sigma_{11}. \tag{43}$$

4.4. Plate in bending loaded in its plane

A plate in bending loaded in its plane (figure 13) is now studied. This is a nonhomogeneous test. The aim of this simulation is to observe different ratios of martensite inside the plate. The volume fraction of martensite ξ depends on the location in the plate. The following pictures show the appearance of the martensite and thus the disappearance of the austenite during the load phase (figures 14, 15 and 16).

It is noticed that the martensite appears around the embedding; then is propagated successively to entirely transform the plate.

The Von Mises stress $\overline{\sigma}$ evolution versus $\overline{\varepsilon}$ is given at a point of the plate which transforms rather quickly (test point A, figure 17). In the same way, the typical pseudoelastic behavior is obtained.

4.4.1. Case of a lengthened plate. In their study, Rejzner *et al* [12] have shown that the neutral fiber of a bending beam does not transform ($\xi = 0$ at each time of the process).

Thus it is interesting to verify this result by using our implementation. The only change to be made is to choose a beam length sufficiently long with respect to its width. Thus, the value of $L = 500$ mm is chosen (figure 18).

Let us recall that for a plate in bending loaded in its plane, the stress tensor can be written as

$$\underline{\sigma} = \begin{bmatrix} \sigma_{11} & \sigma_{12} & 0 \\ \sigma_{12} & 0 & 0 \\ 0 & 0 & 0 \end{bmatrix} \tag{44}$$

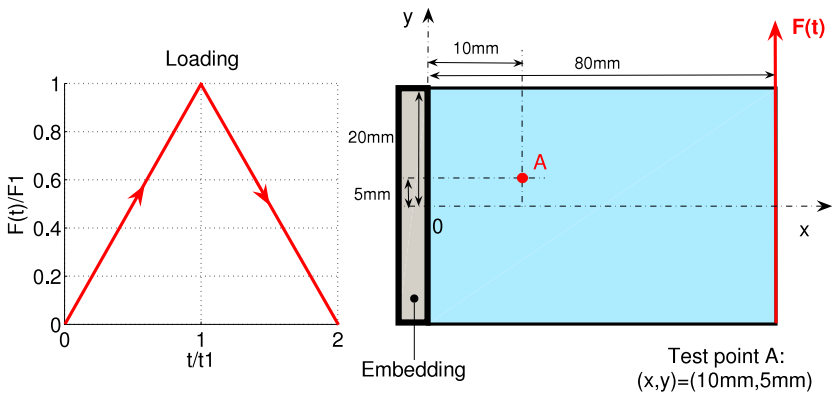

Figure 13. Force loading: plate in bending loaded in its plane.

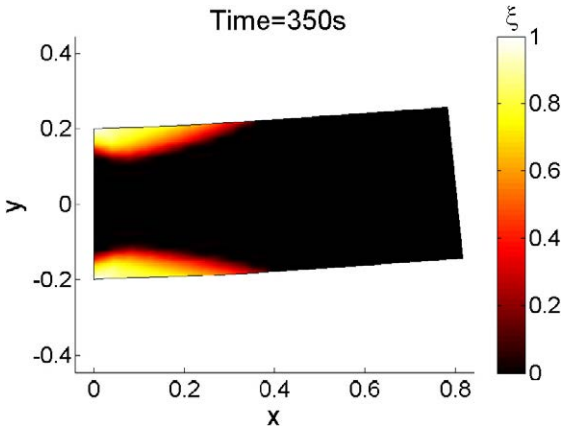

Figure 14. ξ at $t = 350$ s.

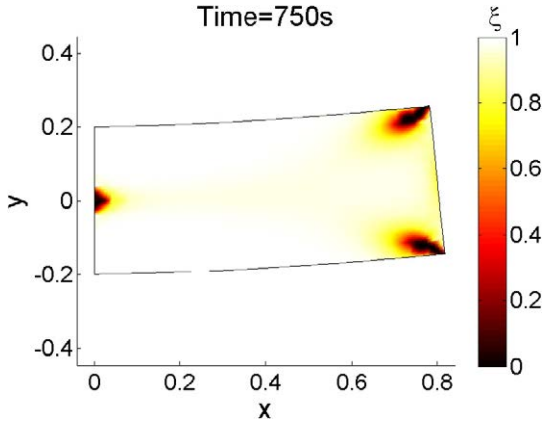

Figure 16. ξ at $t = 750$ s.

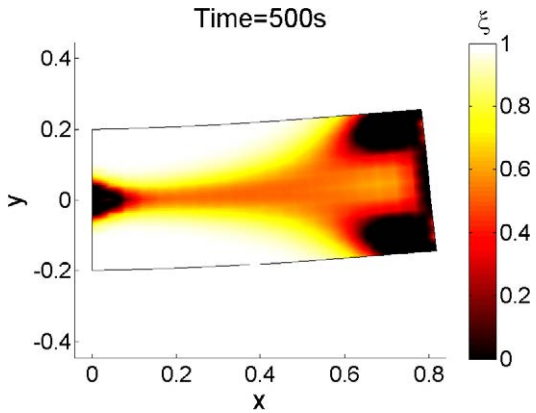

Figure 15. ξ at $t = 500$ s.

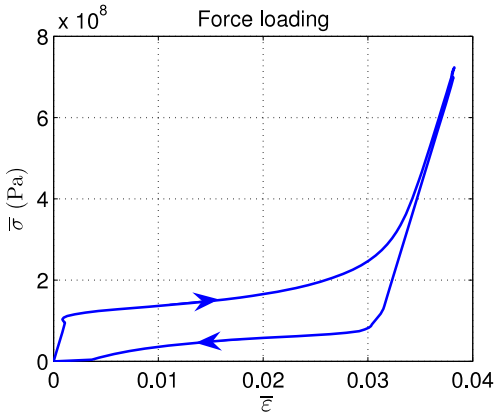

Figure 17. Plate in bending: $\overline{\sigma}$ versus $\overline{\varepsilon}$ at the test point A.

and the elastic solution is

$$\sigma_{11} = y(x-L)\frac{F}{I_{Gz}} \qquad \text{and} \qquad \sigma_{12} = \frac{F}{2I_{Gz}}\left(\frac{l^2}{4} - y^2\right) \tag{45}$$

where I_{Gz} is the quadratic moment of the cross-section around the $(0, \mathbf{z})$ axis.

For a beam, $l \ll L$ implies that σ_{12} is negligible compared to σ_{11}:

$$\left\| \frac{\sigma_{12}}{\sigma_{11}} \right\| \ll 1. \tag{46}$$

So, the stress tensor becomes

$$\underline{\sigma} = \begin{bmatrix} \sigma_{11} & 0 & 0 \\ 0 & 0 & 0 \\ 0 & 0 & 0 \end{bmatrix}. \tag{47}$$

The asymmetry between tension and compression is neglected. Thus, the neutral fiber is localized at $y = 0$. The equation (45) gives $\sigma_{11}(y = 0) = 0$ and thus $\overline{\sigma}(y = 0) = 0$. In consequence, the neutral fiber must never transform. This result is observable in figure 19, obtained at $t = t_1$: in the studied cross-section, all the arc width is transformed ($\xi = 1$) except the neutral fiber ($\xi = 0$) at $y = 0$.

4.5. Internal loops

Internal loops are needed to simulate the dynamic behavior of SMAs (section 5). An internal loop is a loading cycle where the martensite transformation is not complete ($\xi \in [0, 1]$). The criterion of transformation is defined by

$$\pi_{\mathrm{f}}(\overline{\varepsilon}, \overline{\sigma}) = 0. \tag{48}$$

Due to the relation between $\overline{\sigma}$ and $\overline{\varepsilon}$, we have the following system of equations:

$$0 = \frac{\gamma\overline{\sigma}}{\rho} + \pi_{\mathrm{f}}^0 - (1 - 2\xi)\phi_{it} \tag{49}$$

$$\overline{\sigma} = \frac{3E}{2(1+\upsilon)}(\overline{\varepsilon} - \gamma\xi). \tag{50}$$

Thus, we can write an explicit expression for the equation $\pi_{\mathrm{f}}(\overline{\varepsilon}, \overline{\sigma}) = 0$, by eliminating ξ in both equations:

$$\overline{\sigma} = \frac{1}{\frac{4\phi_{it}(1+\upsilon)}{3E\gamma} - \frac{\gamma}{\rho}}\left(\frac{2\phi_{it}}{\gamma}\overline{\varepsilon} + \pi_{\mathrm{f}}^0 - \phi_{it}\right). \tag{51}$$

So, it appears that the transformation points belong to a straight line. In figure 20 there are represented several internal loops and the line of equation (51). For each loop, the transformation points belong to the line which represents $\pi_{\mathrm{f}} = 0$: the state of 'unstable equilibrium'.

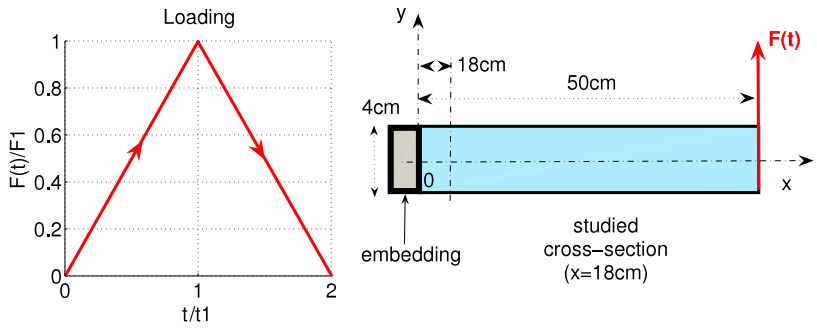

Figure 18. Force loading: beam in bending.

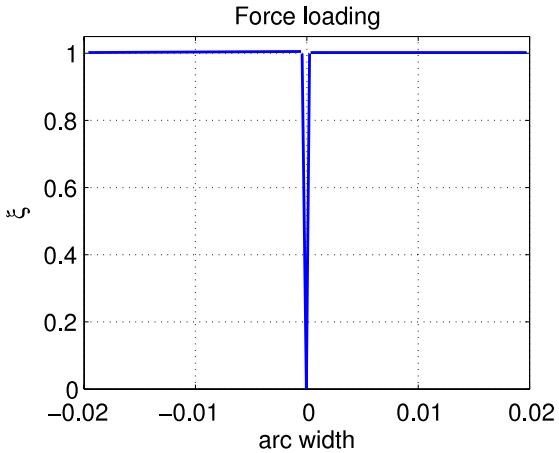

Figure 19. Volume fraction of the martensite in a cross-section ($x = 18$ cm).

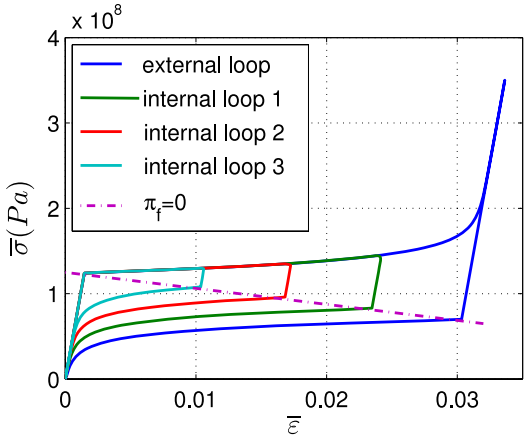

Figure 20. Internal loops and the straight line defined by $\pi_f(\overline{\varepsilon}, \overline{\sigma}) = 0$.

4.6. Assessment of these static tests

By considering the global implementation of the R_I model described in the section 3, many static tests (plate in tension, in proportional bi-tension, in bending loaded in its plane and internal loops) have been investigated. The implementation is practically the same for each simulation: the only changes are in the geometry, the boundary conditions and the material characteristics.

All the results obtained are consistent with the theory background. This implementation will now be used to study the dynamic behavior of SMAs.

5. Dynamic behavior

The mechanical adjustments applied to SMA antiseismic structures can be modeled by some harmonic vibrations (dynamic strains with an amplitude $\overline{\varepsilon}_m$ for a given frequency ω) and a static strain offset $\overline{\varepsilon}_0$. In order to design these devices, it is important to evaluate the influence of $\overline{\varepsilon}_m$ and $\overline{\varepsilon}_0$ on the stiffness and the damping effect of the SMAs. The equivalent complex Young's modulus approach is used to evaluate this influence. It is a powerful tool commonly used in structural dynamics for the characterization of damping materials (damping effect and stiffness). For example, Caracciolo *et al* [13] have characterized a viscoelastic material by determining the equivalent complex Young's modulus of a small beam-like specimen subject to seismic excitation. Gandhi *et al* [6] use this approach in order to characterize the pseudoelastic stress/strain hysteresis damping behavior of an NiTi SMA wire versus the oscillation frequency strain amplitude and the temperature. And finally, Pintelon *et al* have presented in [14] a system identification approach for measuring the elastic modulus of homogeneous viscoelastic materials from longitudinal and flexural vibration experiments, leading to a parametric model for the equivalent complex Young's modulus.

5.1. Equivalent complex Young's modulus

In the mono-axial case, the constitutive relation between σ and ε for a damping material subject to steady state harmonic excitations can be written as

$$\sigma = \overline{E} \cdot \varepsilon = E(1 + i\eta)\varepsilon \tag{52}$$

where $\overline{E}$ is the equivalent complex Young's modulus, E the storage modulus (representation of the stiffness), η the loss factor (representation of the damping). $E\eta$ is usually called the loss modulus. But, first, let us recall the fundamentals of the equivalent complex Young's modulus notion: in order to take into account irreversible effects, the relation between stress and strain must be an operator introducing the concept of behavior differed into time. In 1971, a functional calculus of a general

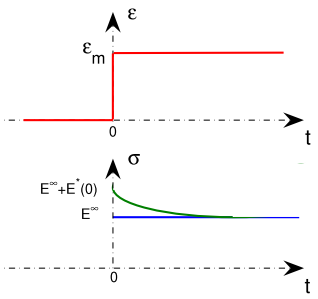

Figure 21. Relaxation test.

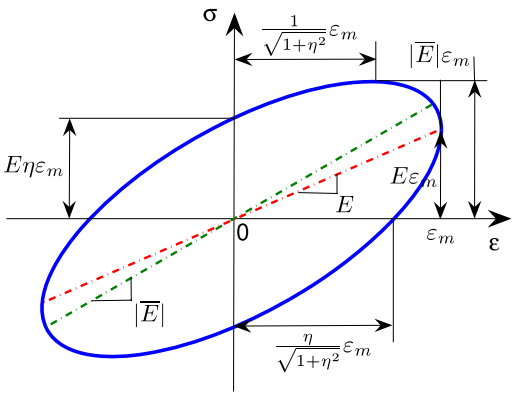

Figure 22. Hysteresis cycle of a damping material, undergoing cyclic strain oscillations of amplitude $\overline{\varepsilon}_{\mathrm{m}}$.

form of behavior laws was proposed by Valanis (endochronic theory) [15]:

$$\sigma(t) = \int_{-\infty}^{t} E(t-\tau)\frac{\mathrm{d}\varepsilon(\tau)}{\mathrm{d}\tau}\,\mathrm{d}\tau \tag{53}$$

where σ is the stress and ε the strain. Let us consider a harmonic strain $\varepsilon(t)$ and $\hat{\varepsilon}(t)$, its Fourier transform:

$$\hat{\varepsilon}(t) = \varepsilon_{\mathrm{m}}\mathrm{e}^{\mathrm{i}\omega t} \qquad \varepsilon(t) = \mathrm{Re}\{\hat{\varepsilon}(t)\}. \tag{54}$$

The relation (53) is linear and should only be applied to linear viscoelastic problems. Furthermore, if the coupling with the temperature T is not taken into account, E is only a function of the time t and can be written as the sum of an asymptotic limit value and a time dependent term:

$$E(t) = E^{\infty} + E^{*}(t) \tag{55}$$

where $E^{*}(t) \to 0$ when $t \to +\infty$. For causality reasons, $E^{*}(t) = 0$ for $t < 0$.

Thus, gathering the relations (55) and (54) into equation (53) leads to

$$\hat{\sigma}(t) = E^{\infty}\varepsilon_{\mathrm{m}}\mathrm{e}^{\mathrm{i}\omega t} + \mathrm{i}\omega\varepsilon_{\mathrm{m}}\int_{-\infty}^{t} E^{*}(t-\tau)\mathrm{e}^{\mathrm{i}\omega\tau}\mathrm{d}\tau. \tag{56}$$

A simple one-dimensional relaxation test allows us to identify E^{∞} and $E(t)$, as shown in figure 21.

With a variable change defined by $\beta = t-\tau$, equation (56) becomes:

$$\hat{\sigma}(t) = \left[E^{\infty} + \mathrm{i}\omega\int_{0}^{\infty} E^{*}(\beta)\mathrm{e}^{-\mathrm{i}\omega\beta}\,\mathrm{d}\beta\right]\varepsilon_{\mathrm{m}}\mathrm{e}^{\mathrm{i}\omega t} \tag{57}$$

which can be written in the Fourier space as

$$\sigma(\omega) = \overline{E}(\omega)\varepsilon_{\mathrm{m}}\mathrm{e}^{\mathrm{i}\omega t}. \tag{58}$$

$\overline{E}(\omega)$ is defined as the equivalent complex Young's modulus. By writing $\mathrm{e}^{-\mathrm{i}\omega\beta} = \cos(-\omega\beta) + \mathrm{i}\sin(-\omega\beta)$, an extensive expression for $\overline{E}(\omega)$ is obtained:

$$\overline{E}(\omega) = \underbrace{E^{\infty}}_{\text{isothermal}} \overset{\text{real}}{+} \underbrace{U(\omega)}_{\text{conservative}} + \mathrm{i}\overset{\text{imaginary}}{\underbrace{V(\omega)}}_{\text{dissipative}} \tag{59}$$

with

$$U(\omega) = \omega\int_{0}^{+\infty} E^{*}(\beta)\sin(\omega\beta)\,\mathrm{d}\beta \tag{60}$$

$$V(\omega) = \omega\int_{0}^{+\infty} E^{*}(\beta)\cos(\omega\beta)\,\mathrm{d}\beta. \tag{61}$$

Finally, the equivalent complex Young's modulus can be written as

$$\overline{E}(\omega) = E(\omega)(1 + \mathrm{i}\eta(\omega)) \tag{62}$$

with the storage modulus E:

$$E(\omega) = E^{\infty} + \omega\int_{0}^{+\infty} E^{*}(\beta)\sin(\omega\beta)\,\mathrm{d}\beta \tag{63}$$

and the loss factor η as

$$\eta(\omega) = \frac{\omega\int_{0}^{+\infty} E^{*}(\beta)\cos(\omega\beta)\,\mathrm{d}\beta}{E^{\infty} + \omega\int_{0}^{+\infty} E(\beta)\sin(\omega\beta)\,\mathrm{d}\beta}. \tag{64}$$

The hypothesis of a hysteretic damping can be stipulated. This assumption entails $E(\omega) = E$ and $\eta(\omega) = \eta$; thus

$$\overline{E} = E(1 + \mathrm{i}\eta). \tag{65}$$

Assuming that equation (65) is verified, the harmonic strain input $\varepsilon(t)$ and the corresponding stress $\sigma(t)$ are evaluated as

$$\varepsilon(t) = \mathrm{Re}\{\hat{\varepsilon}(t)\} = \varepsilon_{\mathrm{m}}\cos(\omega t) \tag{66}$$

$$\sigma(t) = \mathrm{Re}\{\hat{\sigma}(t)\} = E\varepsilon_{\mathrm{m}}(\cos\omega t - \eta\sin\omega t). \tag{67}$$

A graphical representation of both equations (66) and (67) in the (ε, σ) axis system yields the classical stress/strain elliptical hysteresis cycle of a damping material subjected to harmonic excitations of amplitude ε_{m} (figure 22).

For the multi-axial situation, the same reasoning can be developed with the equivalent stress and strain $(\overline{\sigma}, \overline{\varepsilon})$.

5.2. Equivalent complex Young's modulus: application to SMA.

This equivalent complex Young's modulus concept will now be used to describe the nonlinear dynamic behavior of SMAs. Although this concept supposes a linear viscoelastic behavior of the material, this mathematical tool can be generalized to quantify the response on the first harmonic of a material having a nonlinear hysteretic behavior.

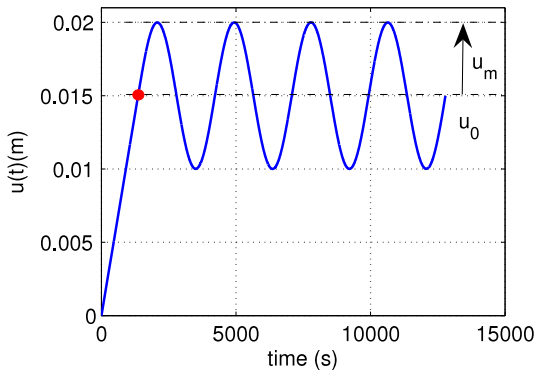

Figure 23. Command function (displacement loading) for a plate in tension.

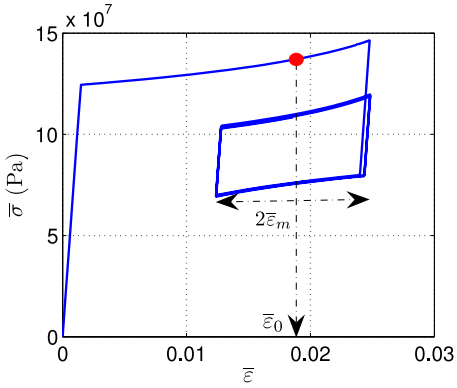

Figure 24. SMA response due to the command function given in figure 23.

Let us consider that the specific potential (E_p) and strain (E_d) energies stored during a period of request are calculated:

$$E_\mathrm{p} = \int_0^T \sigma \cdot \dot{\varepsilon}\, \mathrm{d}t \tag{68}$$

$$E_\mathrm{d} = \int_0^T \sigma \cdot \varepsilon\, \mathrm{d}t. \tag{69}$$

For a nonlinear material loaded in a cyclic strain (equation (66)), E_p and E_d are evaluated as

$$E_\mathrm{p} = \varepsilon_\mathrm{m} \int_0^T \sigma(t) \cos \omega t\, \mathrm{d}t \tag{70}$$

$$E_\mathrm{d} = -\omega \varepsilon_\mathrm{m} \int_0^T \sigma(t) \sin \omega t\, \mathrm{d}t \tag{71}$$

and for a linear viscoelastic material, due to the relation (66)–(68), E_d and E_p are linked to E and η by

$$E_\mathrm{p} = \frac{\pi E \varepsilon_\mathrm{m}}{\omega} \tag{72}$$

$$E_\mathrm{d} = \pi E \eta \varepsilon_\mathrm{m}. \tag{73}$$

Energy equivalence envisages equality between the specific potential and strain energies of the two material types. Thus, the storage modulus E and the loss factor η are made explicit by both equations (74) and (75):

$$E = \frac{\omega}{\pi \varepsilon_\mathrm{m}} \int_0^T \sigma(t) \cos \omega t\, \mathrm{d}t \tag{74}$$

$$E\eta = \frac{-\omega}{\pi \varepsilon_\mathrm{m}} \int_0^T \sigma(t) \sin \omega t\, \mathrm{d}t. \tag{75}$$

Again, these results can be generalized to the multi-axial cases by considering the equivalent Von Mises stress and strain.

5.3. Results

A plate in tension loaded in displacement by the command function given in figure 23 is performed. A vibration state (amplitude $\overline{\varepsilon}_\mathrm{m}$) is established around a static strain offset ($\overline{\varepsilon}_0$). This static strain offset is reached linearly. The response of the SMA is given in figure 24.

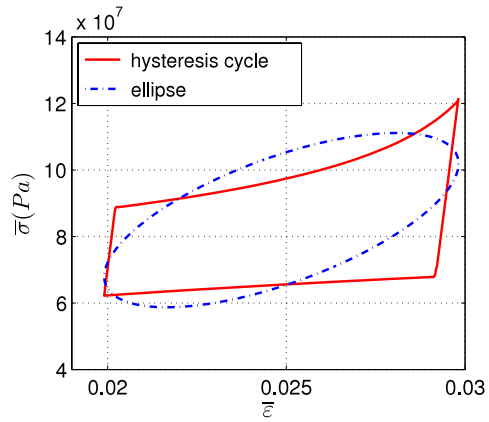

Figure 25. Hysteresis cycle and corresponding ellipse for $\overline{\varepsilon}_0 = 0.025$ and $\overline{\varepsilon}_\mathrm{m} = 0.005$.

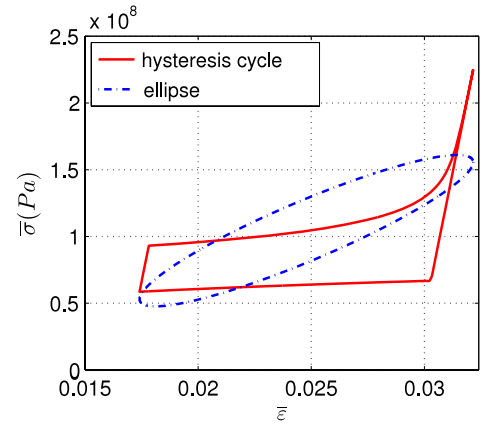

Figure 26. Hysteresis cycle and corresponding ellipse for $\overline{\varepsilon}_0 = 0.025$ and $\overline{\varepsilon}_\mathrm{m} = 0.007$.

The last cycle is then preserved to evaluate the storage modulus E and the loss factor η by using equations (74) and (75) and the corresponding ellipse defined by equations (66) and (67). Many cycles were simulated with different values of $\overline{\varepsilon}_\mathrm{m}$ and $\overline{\varepsilon}_0$. Figures 25–27 show the stabilized cycles and the corresponding ellipse for the static strain offset $\overline{\varepsilon}_0 = 0.025$ and three different strain amplitudes.

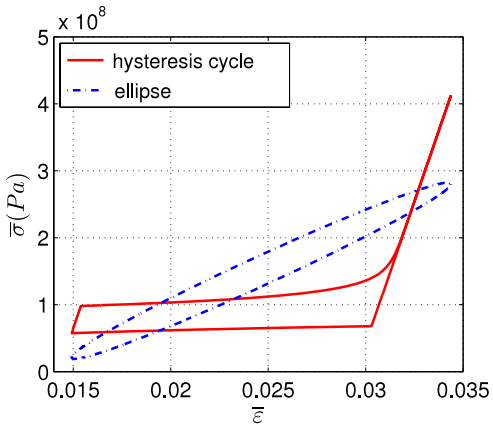

Figure 27. Hysteresis cycle and corresponding ellipse for $\overline{\varepsilon}_0 = 0.025$ and $\overline{\varepsilon}_{\mathrm{m}} = 0.01$.

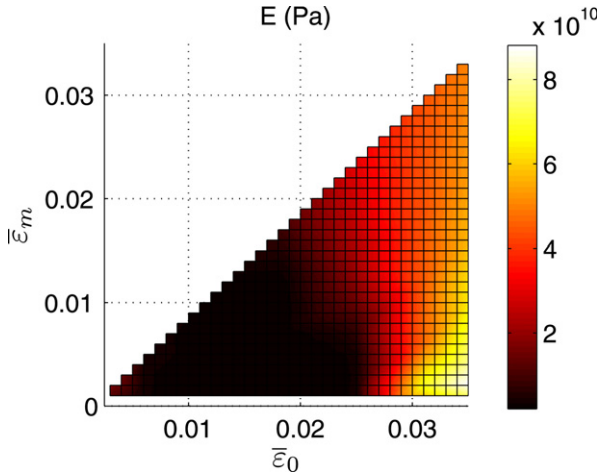

Figure 28. Storage modulus: E versus $(\overline{\varepsilon}_0, \overline{\varepsilon}_{\mathrm{m}})$.

Table 2. E and η versus $\overline{\varepsilon}_{\mathrm{m}}$ for $\overline{\varepsilon}_0 = 0.025$.

$\overline{\varepsilon}_{\mathrm{m}}$	E	η
0.005	34×10^8	1.17
0.007	69×10^8	0.46
0.01	133×10^8	0.18

Thus, the values of E and η for these three cases are listed in table 2.

Clearly, for small cyclic strain amplitudes, the ellipses are fairly close to the cycles, suggesting that the complex modulus representation of the SMA material behavior is quite accurate. For larger strain amplitudes, however, considerable differences can be seen between the hysteresis cycle and the corresponding ellipse, due to the fact that the behavior becomes strongly nonlinear.

Finally, the graphic representation of the storage modulus E and the loss factor η versus the static strain offset $\overline{\varepsilon}_0$ and the strain amplitude $\overline{\varepsilon}_{\mathrm{m}}$ are respectively given in figures 28–31.

The simulations seem to be good from a qualitative point of view. Indeed, as the static strain offset increases, a rapid increase of the storage modulus is noticed. The elastic behavior

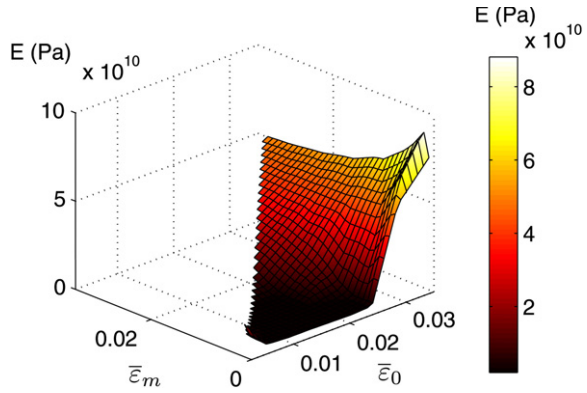

Figure 29. Storage modulus: E versus $(\overline{\varepsilon}_0, \overline{\varepsilon}_{\mathrm{m}})$ represented in three dimensions.

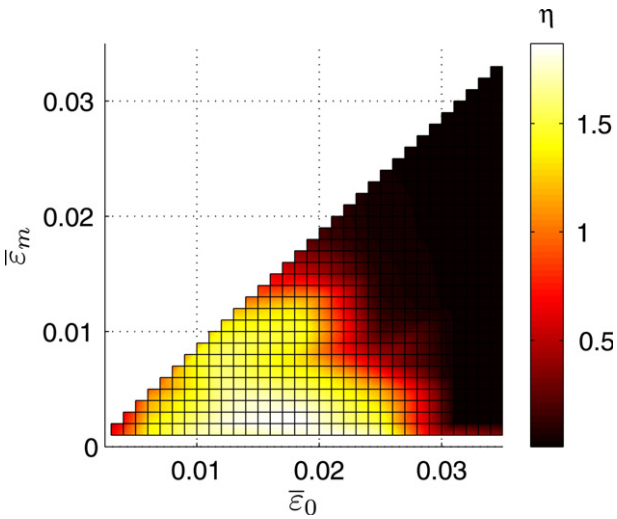

Figure 30. Loss factor: η versus $(\overline{\varepsilon}_0, \overline{\varepsilon}_{\mathrm{m}})$.

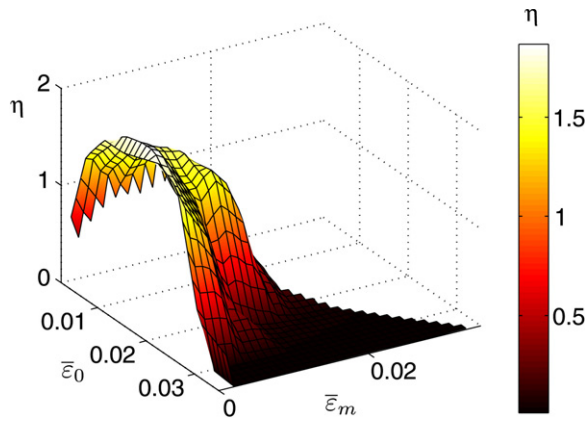

Figure 31. Loss factor: η versus $(\overline{\varepsilon}_0, \overline{\varepsilon}_{\mathrm{m}})$ represented in three dimensions.

zone of the martensite is reached when the static strain offset exceeds 3%.

With static strain offsets between 0.1% and 3% (the pseudoelastic behavior zone), the storage modulus is minimal. This observation is consistent because of the presence of the

plateau of the martensitic transformation. In this zone, the stiffness is negligible compared to those noticed in the elastic behavior zones of the austenite and martensite. In the same way, still with static strain offsets between 0.1% and 3%, the loss factor is maximal, which confirms that the damping effect is due to the martensitic transformation end the pseudoelastic behavior. Above 3%, the loss factor decreases and becomes quickly negligible. This effective decrease is consistent with the fact that there is no damping effect in the elastic behavior zone of the martensite. The same observation can be made with the static strain offsets lower than 0.1% (elastic behavior zone of the austenite).

Higher damping is obtained in the pseudoelastic behavior zone and for small cycle strain amplitudes. Indeed, a decrease of the loss factor is obtained with an increase of the cyclic strain amplitude. This is consistent with the fact that in this zone, the SMA behavior is totally pseudoelastic (figure 27) for small strain amplitudes; for more significant strain amplitudes, the SMA behavior is partially pseudoelastic and elastic (figure 25), leading to a loss of damping.

6. Conclusions

In this paper, the characterization of the dynamic behavior of shape memory alloys versus two parameters—the strain amplitude and the static strain offset—has been performed by using the equivalent complex Young's modulus approach.

In the first part, a phenomenological model (R_I model) has been implemented in COMSOL© in order to simulate internal loops for many cases of displacement loadings.

In the second part, for checking the implementation, many static tests have been performed: plate in tension, in proportional bi-tension, in bending loaded in its plane.

In the third part, the equivalent complex Young's modulus has been presented. Many cases of displacement loadings with different values of the static strain offset and the strain amplitude have been simulated.

Finally, the storage modulus and the loss factor have been calculated. Thus, this study allows us to highlight the existence of a high damping zone which is localized for static strain offsets between 0.1% and 3% and small strain amplitudes (the totally pseudoelastic behavior zone of the SMA). This new modeling tool allows us to improve the nonlinear modeling of SMAs in order to develop and optimize applications for control and damping in civil engineering.

References

[1] Raniecki B, Lexcellent C and Tanaka K 1992 Thermodynamic models of pseudoelastic behavior of shape memory alloys *Arch. Meh.* **44** 261–84

[2] Bono F and Tirelli D 1999 Characterisation of materials for the innovative antiseismic techniques. Results of the experimental campaign performed at the JRC ISPRA on samples of smas *Internal Report* ELSA Laboratory

[3] Tirelli D, Renda V and Bono F 2000 Characterisation of shape memory alloys applications to the retrofitting of brick masonry wall by the pseudo-dynamic method and numerical models *Internal Report* ELSA Laboratory

[4] Magonette G, Marazzi F, Molina J and Renda V 2000 Structural control: experimental activity at ELSA *Internal Report* ELSA Laboratory

[5] Collet M, Foltete E and Lexcellent C 2001 Analysis of the behavior of a shape memory alloy beam under dynamical loading *Eur. J. Mech.* A **20** 615–30

[6] Gandhi F and Wolons D 1999 Characterization of the pseudoelastic damping behavior of shape memory alloy wires using complex modulus *Smart Mater. Struct.* **8** 49–56

[7] Raniecki B and Lexcellent C 1998 Thermodynamics of isotropic pseudoelasticity in shape memory alloys *Eur. J. Mech.* A **17** 185–205

[8] Marbuger R E and Koistinen D P 1959 A general equation prescribing the extent of the austenite–martensite transformation in pure non-carbon alloys and plain carbon steels *Acta Metall.* **7** 55–69

[9] Lexcellent C and Rejzner J 1998 Modeling of the strain rate effect, creep and relaxation of a Ni–Ti shape memory alloy under tension (compression)–torsional proportional loading in the pseudoelastic range *Smart Mater. Struct.* **9** 613–21

[10] Berton O 2002 Education multi axiale des alliages memoire de forme *DEA 857* Universite de Fanche-Comte

[11] Bouvet C 2001 De l'uniaxial au multiaxial: comportement pseudoelastique des alliages a memoire de forme *Thesis 870* Universite de Fanche-Comte

[12] Rejzner J, Lexcellent C and Raniecki B 2001 Pseudoelastic behaviour of shape memory alloy beams under pure bending: experiments and modelling *Int. J. Mech. Sci.* **44** 665–86

[13] Caraciolo R, Gasparetto A and Giovagnoni M 2004 An experimental technique for complete dynamic characterization of a viscoelastic material *J. Sound Vib.* **272** 1013–32

[14] Pintelon R, Guillaume P, Vanlanduit S, De Belder K and Rolain Y 2004 Identification of Young's modulus from a broadband modal analysis experiment *Mech. Syst. Signal Process.* **18** 699–726

[15] Valanis K C 1971 A theory of viscoplasticity without a yield surface *Arch. Mech. Stosow.* **23** 517–51